

USE OF CFD TO CORRELATE CRUDE OIL FOULING AGAINST SURFACE TEMPERATURE AND SURFACE SHEAR STRESS IN A STIRRED FOULING APPARATUS

Mengyan Yang*, Andrew Young and Barry Crittenden
Department of Chemical Engineering
University of Bath, Bath, UK, BA2 7AY

*corresponding author: my223@bath.ac.uk

ABSTRACT

Experimental data on the fouling of various crude oils is being obtained in a small (1 litre) batch stirred cell which is operated at temperatures up to 400°C and pressures up to 30 bar. The cell is based on the Eaton and Lux patented design. The fouling resistance is found to increase more-or-less linearly with time after an induction period. Distributions of shear stress, surface temperature and heat flux over the cell's heated test finger are modelled using the Comsol CFD package. The CFD simulation results are validated against the measured temperature data at various axial positions on the heated test probe. At the end of a fouling run, the cell is dismantled and the fouling layer thickness is measured using the Proscan technique. The profile of fouling layer thickness along the heated surface is found to be in an almost parabolic form, with its maximum thickness near to the middle of the surface. The CFD-predicted surface temperature profiles are strikingly similar whilst the predicted shear stress profiles are found to be virtually flat. Hence, it becomes possible to correlate, for a fixed surface shear stress, the local fouling rate against the local surface temperature, and hence to obtain an Arrhenius plot from one experimental run. The local experimental shear stress can be varied by changing the speed of rotation of the cell's cylindrical stirrer and so the effect of shear stress on fouling behaviour can be studied as well.

INTRODUCTION

Eaton and Lux (1983, 1984) designed a batch stirred cell system and carried out experiments over the pressure range 3-20 bar with test-probe surface temperatures up to 600°C. It was claimed that very good simulations could be obtained of actual fouling situations and the apparatus was applied to a wide variety of crude oils and operating conditions. This type of experimental apparatus is relatively compact, can even be made portable, and uses much less volume of crude oil for experiments than recirculating flow loops (Crittenden et al., 2009). Moreover, the batch stirred cell can easily be dismantled for inspection of the fouling layer after test runs, permitting easy extraction of samples for analysis without destruction of any of its parts. The experimental operation with the batch stirred cell is relatively straightforward and faster than with a recirculating flow loop system. In this work, therefore, a batch stirred cell

system has been constructed based on information in the original patent (Eaton, 1983) and used to obtain fundamental experimental data with selected crude oil samples.

Despite the advantages just mentioned, the potential application of the batch stirred cell could be limited by three factors. Firstly, the surface temperature of the heated probe could be difficult to obtain reliably because it needs to be estimated from the reading of thermocouples which are embedded within the heated probe. Thus, estimation of the temperature of the clean heat transfer surface, and subsequently of the deposit-fluid interface, could be questionable at locations some distance away from the thermocouples. Secondly, there is a lack of knowledge of the shear stress distribution over the heated probe surface where fouling layer builds up. Much more knowledge is usually available for fluid flow inside a round tube than for rotating turbulent fluid flow on the outside of a heated test probe in the batch cell. Thirdly, measurement of the thickness of the foulant layer may not be straightforward even though the deposit is formed on the outside surface of a heated test finger.

In order to improve the reliability of the surface temperature measurement, it is possible to place measurement thermocouples near to, but not actually on, the surface on which deposits form. Indeed, it is possible to place a number of such thermocouples at different locations along and around the test probe surface. A possible solution to the first and second factors is to compliment experimental heat transfer measurements with CFD simulation. In the present study a commercial CFD software package, Comsol (Comsol Inc, Burlington, MA, USA), has been used to model the distributions of fluid velocity, shear stress, surface temperature and heat flux over the batch stirred cell's heated test probe. The Comsol CFD package is capable of modeling fluid dynamics and heat transfer in the turbulent flow regime using either the k- ϵ or the k- ω model, and offers user-friendly graphic interfaces for the fluid property and boundary condition settings. Some of the CFD simulation results, notably temperature, can be validated against the measured temperature data at various axial positions on the heated test probe.

Eaton and Lux (1984) assumed, however, that there was a uniform temperature over the probe surface. Moreover,

they used the net weight of the fouling deposit as a key measure of the fouling severity/rate over a given period of time. The Eaton and Lux approach therefore did not take into account that there could well be a distribution not only of surface temperature on the heated probe but distributions of surface shear stress and fouling layer weight/thickness as well. To obtain the accurate weight of foulant deposited unevenly over the probe surface would be virtually impossible because small amounts of deposit removed locally could not be made without loss and hence could not be made accurately. In order to overcome this deficiency in the present study, Proscan 2000, a micro-optical scanning technique developed by Scantron Industrial Products Ltd, Taunton, England, has been utilized to measure the fouling layer thickness locally on the heated test probe surface once the test probe has been removed from the batch cell. The principal advantages of Proscan 2000 are the high resolution of surface profiles which can be obtained at micro levels, and easy alignment of the surface that is being scanned.

Given now that (i) local fouling rates can be obtained from local thermocouple data when the batch cell is operated at constant heat flux and constant average turbulence intensity, (ii) the local fouling layer thickness profile developed over a given time period can be obtained using Proscan 2000, and (iii) the local surface temperature and shear stress profiles can be obtained from CFD simulations using Comsol, a large amount of scientific information about the fouling process can be obtained from a reduced number of experiments with the batch stirred cell.

EXPERIMENTS, PROSCAN MEASUREMENT AND CFD SIMULATION

Fouling Experiments

A general arrangement of the batch stirred cell is shown in Figure 1. Details of its construction and operation are provided by Young et. al. (2009). The cell comprises a pressure vessel, an upwards pointing test probe heated internally by a cartridge heater, a cylindrical stirrer mounted co-axially with the test probe and driven via a magnetic drive by an electric motor, an internal cooling coil, external surface band heaters, and a pressure relief system. There is a single thermocouple, t_{bulk} , to measure the crude oil bulk temperature and two thermocouples, t_{wb} and t_{ws} are located within the walls of the test probe. Operating experience has shown that the fouling rate is normally linear, perhaps after an induction period, and since the heated probe is operated at constant heat flux, the local fouling rate can be found from the gradient of the plot of surface temperature against time (Crittenden et al., 2009).

At the centre of the cell, the upward pointing heated probe is set into the base from which it can be removed at the end of a fouling experiment for observations of the deposit and measurements of deposit thickness. The probe is made of low carbon steel with a material specification similar to that of a standard A179 heat exchanger tube.

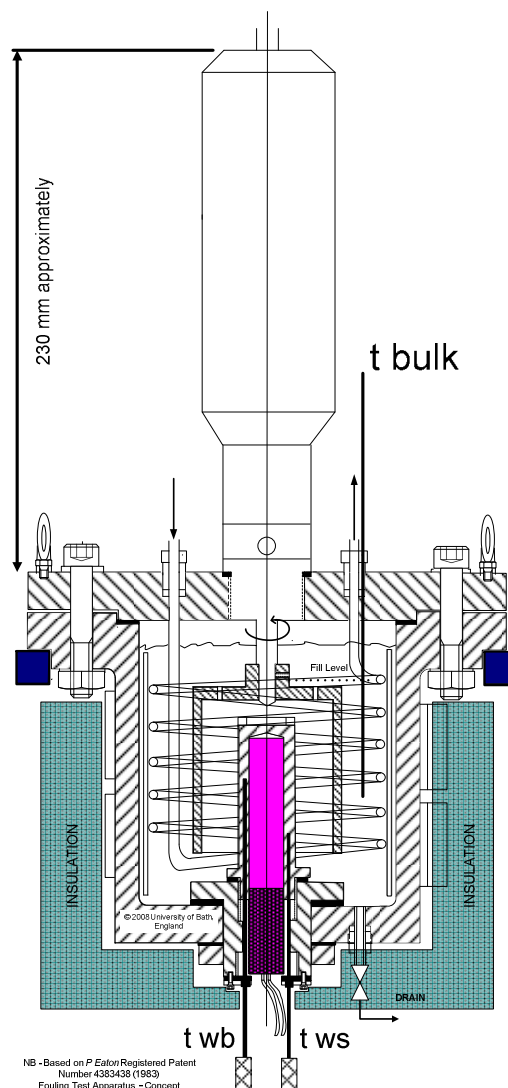


Fig. 1 The stirred cell system

Thermocouples: t_{bulk} to measure bulk temperature T_{bulk} ; t_{wb} and t_{ws} to measure the probe temperature T_{wb} and T_{ws} respectively

The cell is filled with about 900 mL of the crude oil, pressurized with nitrogen, and stirred using the 60mm OD coaxial cylinder driven by the electric motor. There are two heat sources in the system, one being the cartridge heater located in the centre of the probe, the other being electric band heaters attached around the outside wall of the pressure vessel. The side and the bottom surfaces of the cell are well insulated. The bulk temperature is maintained constant using a PID controller that regulates the coolant flow through the cooling coil. The coolant enters from the bottom and leaves from the top. When the bulk temperature reached the set point, the pressure is normally about 20bar. The temperature of the probe surface depends on both the power input to the cartridge heater and the bulk temperature. The real time data of temperature, probe heating power, and the stirring speed are acquired on-line using LabVIEW™ 8 (National Instruments, USA).

Proscan Measurement

At the end of a fouling run the cell is cooled and the probe is removed. Figure 2 shows a probe with a typical fouling deposit. The probe is placed in a vacuum oven to allow any liquid oil residue to evaporate off. It is then held with a V block and placed in the measuring plate of the Proscan 2000. The surface of the probe is scanned using a laser optical sensor to measure the fouling layer thickness profile.



Fig. 2 The heated test probe partially covered with deposit

CFD Simulation

CFD and heat transfer simulations are carried out using Comsol Version 3.4. The flow mode needs to be determined prior to the simulation. A number of publications report that the fluid flow between two concentric cylinders with one rotating becomes turbulent even at low or moderate rotational speeds (Mullin et al., 1982, Smith and Townsend, 1982, Churchill, 1988). To confirm the flow mode visually, a model cell of a similar size was built using a glass beaker as the cell body, and transparent polycarbonate material as the rotating cap and the central probe. Tests using water containing small particles as the fluid showed that the flow was turbulent even at a rotating speed as low as 100rpm. Given that the viscosity of water at room temperature is similar to that of crude oil at about 250°C, the flow conditions in the model plastic cell would be similar to those of the crude oil in the batch stirred cell under typical fouling test conditions. As all fouling experiments are normally carried out with a stirring speed in excess of 100rpm, the CFD simulation is always conducted using a turbulent model. Because of the swirl flow feature, the Realizable k-ε model is selected for the simulation.

The basic equations of the k-ε turbulent flow model are now described. The equation of continuity and the equation of momentum are in similar forms to normal Navier-Stokes equations but with the addition of the turbulent dynamic viscosity term to the viscosity expression. The equations of the turbulent kinetic energy (k) and the dissipation rate of

turbulent energy (ε) are as follows (Comsol, 2006a; Wilcox, 2000):

$$\frac{\partial(\rho k)}{\partial t} + \rho u \cdot \nabla k = \nabla \cdot \left[\left(\eta + \frac{\eta_T}{\sigma_k} \right) \nabla k \right] + \eta_T [\nabla u + (\nabla u)^T] - \rho \varepsilon \quad (1)$$

$$\frac{\partial(\rho \varepsilon)}{\partial t} + \rho u \cdot \nabla \varepsilon = \nabla \cdot \left[\left(\eta + \frac{\eta_T}{\sigma_\varepsilon} \right) \nabla \varepsilon \right] + \rho C_{\varepsilon 1} C_\mu k [\nabla u + (\nabla u)^T] - \rho C_{\varepsilon 2} \frac{\varepsilon^2}{k} \quad (2)$$

Here, $\eta_T = \rho C_\mu k^2 / \varepsilon$ is the turbulent dynamic viscosity. Values of the k-ε model parameters are given as follows (Comsol 2006b):

$$C_\mu = 0.09 \quad (3)$$

$$C_{\varepsilon 1} = 1.44 \quad (4)$$

$$C_{\varepsilon 2} = 1.92 \quad (5)$$

$$\sigma_k = 1.0 \quad (6)$$

$$\sigma_\varepsilon = 1.3 \quad (7)$$

These equations describe the fluid flow under its steady state. Initially, the fluid passes through a transient period until reaching the steady state. At the end of this period, the gas and liquid interface becomes steady. Comsol is capable of modeling this transient period, although it requires a much longer running time. Once the steady phase interface has been established, the simulation is carried out with the stationary solver. For the heat transfer equations, the turbulence results in an effective thermal conductivity k_{eff} (Comsol, 2006a):

$$k_{eff} = k_o + k_T \quad (8)$$

$$k_T = C_p \eta_T \quad (9)$$

For the purposes of simplicity, the batch stirred cell geometry is taken to be two-dimensional with axial symmetry. Justification for this simplification is made later in the paper. The model tree consists of the turbulent swirl flow, heat conduction and convection in the fluid phase including the moving cap together with heat conduction in the stationary phases. The boundary conditions are now described. For the swirl flow there are logarithmic wall functions for the fluid and wall, for the moving wall for the fluid and for the rotating stirrer wall. For the heat transfer, there is a thermal wall function for the fluid side and a heat flux for the wall side. The heat flux through the wall of the heated probe was set according to the power supplied. The logarithmic wall function is used to model the fluid flow near the walls. This is the Comsol default setting for the turbulent flow. According to Comsol, this empirical relationship is often used over a wide range of Reynolds numbers with reasonable accuracy.

The physical property data for each crude oil are obtained from the supplier and from the literature (ASTM D341, 2003, Nelson, 1958). Comsol software has a built-in library for the physical properties of the more common materials, such as the steel and nitrogen.

RESULTS AND DISCUSSIONS

Typical Fouling Curve

Fouling experiments using the batch stirred cell have been carried out using a number of crude oil samples including those supplied by Petronas and Exxon-Mobil. Operating conditions have been in the range of 300 - 400°C for surface temperature, 200 - 280°C for bulk temperature, and 100 - 400rpm for the rotational stirrer speed which corresponds to a Reynolds number range of about 6000 to 30000. The method for calculation of the fouling resistance based on the temperature measurements can be followed in the publications of Asomaning and Watkinson (2000) and Crittenden et. al. (2009). The fouling test results of crude oil known as Petronas B are reported and correlated with the CFD simulation in this paper. Figure 3 shows data from a typical fouling run with a stirring speed of 200 rpm (3.33 Hz), a bulk temperature of 260°C, a probe heating power of 500W which corresponds to a heat flux of 106 kW/m². More fouling experimental results using the batch stirred cell are presented by Young et. al. (2009).

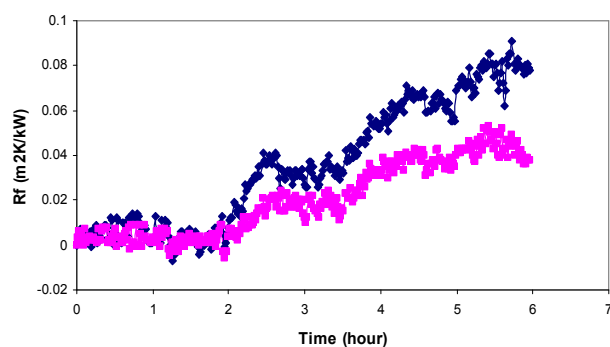


Fig. 3 Typical fouling resistance curve for Crude B crude oil (average heat flux: 106kW/m²; surface temperatures: ■: 376°C; ◆: 385°C)

The surface temperatures are estimated based on the readings of the embedded thermocouples embedded within the walls of the test probe. The results shown in Figure 3 show the initial fouling behaviour starting with a freshly cleaned test probe. The fouling curves reveal that there was an induction period in both cases. This is consistent with the observations of Eaton and Lux (1984). The fouling experimental runs could be stopped at the end of a day and re-started the next day, and so on. The results from many runs have shown that by operating the batch stirred cell in this manner, the fouling curves continue without discontinuity despite the discontinuity of the running time. Indeed, the fouling rate remains almost linear when the test cell is operated in this way, providing a further advantage in that shift working is not required in the laboratory in order to obtain fouling resistance data over extended periods of time. The fouling rates shown in Figure 3 were calculated to be 0.016m²K/(kWh) at a surface temperature of 385°C and

0.011m²K/(kWh) at 376°C. A fouling experiment using a higher stirring speed of 400 rpm (6.67 Hz) and the same surface temperature of 385 °C resulted in a lower fouling rate of 0.0054m²K/(kWh). The effect of the stirring speed, and hence of the shear stress, on the fouling rate will be discussed in the next section.

CFD and Heat Transfer Simulation

The initial transient simulation was carried with a time dependence solver with the time step set to be 0.01second. The results showed that the gas/liquid interface became steady after 3.6 seconds. The simulation of this transient period took about 1.5 hours. The simulation was then carried out to obtain the steady state solution. It should be noted that fouling is so slow that even when it does occur, a pseudo thermal steady state can be assumed at any point in time, and here the steady state solution refers to the case when the fluid flow and temperature field just become stable. Figure 4 shows the velocity field and the gas and liquid interface which is leaning toward the wall as expected for the swirl flow. For simplicity, the six white circles near the wall represent the coiling coil and the small gap in the top of rotating stirrer represents one of its four vent holes. Otherwise, the geometry would need to be three-dimensional, thereby making the simulation much more complicated and hence more time consuming. The steady state simulation usually takes about 30 minutes of computational time.

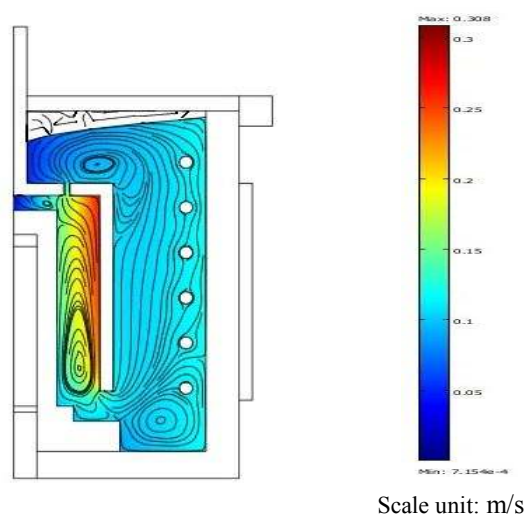


Fig. 4 Velocity field (crude oil: Crude B; stirring speed: 200 rpm; probe heating power: 500W, corresponding to an average heat flux of 106 kW/m²; bulk temperature: 260°C;

Figure 5 shows the CFD-simulated temperature distributions in both the solid and fluid phases for Petronas B crude oil with the operating conditions shown in the caption to Figure 4. The temperature of the bulk of crude oil was relatively even, at about 530K (257°C) in comparison with the set point of 260°C. Figure 6 shows the temperature distribution over the probe surface and over the radius position where the two surface (wall) thermocouples, denoted by T_{wb} and T_{ws} , are located. The good agreement

between the actual measurements for T_{wb} and T_{ws} and their model predicted values using Comsol helps to validate the simulation.

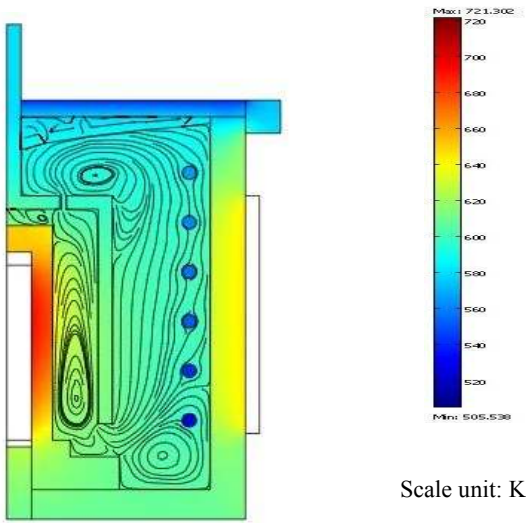


Fig. 5 Temperature distribution with Crude B

Justification for Using Two Dimensional Simplification

The coil strictly makes the geometry three dimensional. Figure 6a shows a three-dimensional CFD simulation for the flow field of the experiment exactly the same as shown in Fig. 4, which applies to all the 3-D figures below. Here, the coil is represented accurately and hence is a true three-dimensional representation of the apparatus. Figure 6b shows the three-dimensional CFD simulation when the coil is simplified to consist of six identical and uniformly spaced circles, which can be accurately represented by the 2-D axial symmetrical geometry. It can be seen that there is no difference between the CFD predictions inside the rotating cylinder for these two cases. It is the conditions within the rotating cylinder which are the most important since the fouling occurs on the hot probe in the centre. The corresponding comparison for the temperature fields is shown in Figs 7a and 7b. Again, it can be seen that there is no difference between the CFD predictions inside the rotating cylinder for these two cases.

Figures 8a and 8b show CFD predictions for a horizontal slice for the 3-D simulation with the actual coil. Axial symmetry is clearly demonstrated, particularly inside the rotating cylinder, the region of most relevance to the fouling. Table 1 shows typical predicted values for velocity and fluid temperature at different locations in the region inside the rotating cylinder. It is clear from the Figures and Table 1, therefore, that the axially symmetrical 2-D simulation is an accurate simplification of the 3-D situation even when the coil is represented accurately. The axially symmetrical 2-D simplification reduces the computing time by a factor of 1/30.

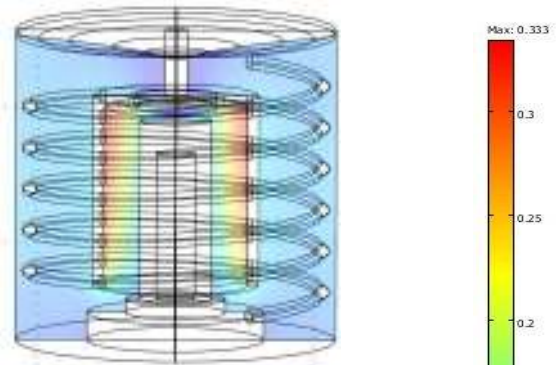


Fig. 6a 3D velocity field – helical coil

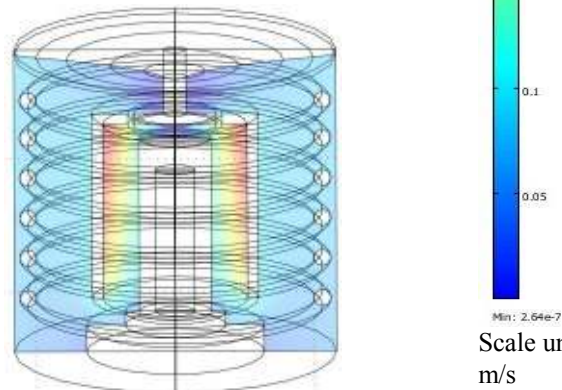


Fig. 6b. 3D velocity field – circular coils

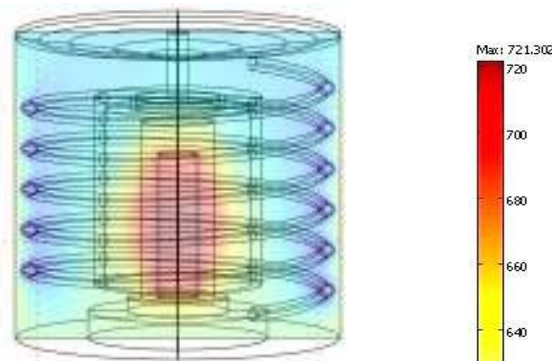


Fig. 7a 3D temperature field – helical coil

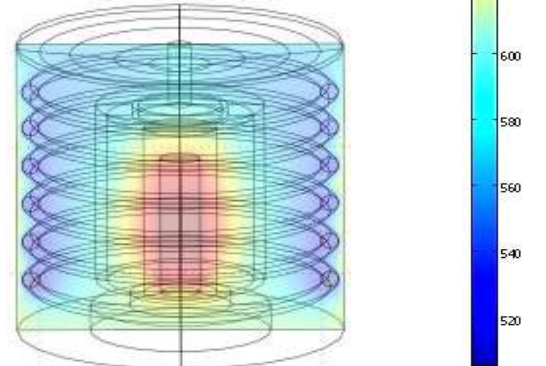


Fig. 7b 3D temperature field – round coils

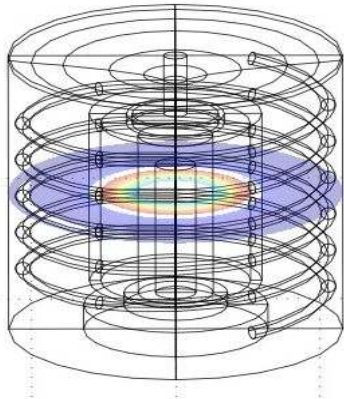


Fig. 8a 3D velocity field with helical coil, $r - \phi$ slice

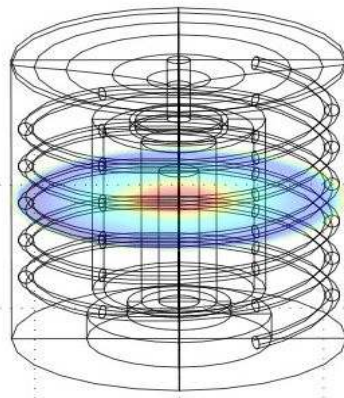


Fig. 8b 3D temperature field with helical coil, $r - \phi$ slice

Table 1 Comparison of 3-D and Axially Symmetrical 2-D Simulations

Location (r, z, ϕ)	Variable	3D simulation	2D simulation
0.0131, 0.04, 0.5π	Velocity	0.115 m/s	0.119 m/s
0.0131, 0.04, 0.75π	Velocity	0.113 m/s	0.119 m/s
0.015, 0.03, 0.25π	Temperature	568 K	570 K
0.015, 0.03, 0.5π	Temperature	567 K	570 K

For comparison, the simulation using the $k-\omega$ model resulted in virtually the same predicted values of velocity and temperature as the Realizable $k-\epsilon$ model. All the simulation data reported below are of the simulation using the Realizable $k-\epsilon$ model.

Figure 9 shows the CFD predicted distribution of probe surface temperature (blue line) and the temperature distribution at the radial position (0.010 m) (red dashed line) where the thermocouples are located along the length (z) of the heated test probe. The two temperature measurements agree very well with the predicted values in terms of their magnitude at their particular locations. The two probe temperature measurements are denoted by \bullet for T_{wb} and \blacksquare for T_{ws} . Table 2 shows more data which helps to validate the CFD simulation.

As shown in Fig. 10, the Comsol-simulated distribution of heat flux over the probe surface length was relatively flat over a 50mm vertical length in the central region. The lower heat fluxes towards the ends of the heated surface are as expected. Indeed, the lower surface temperatures created by the lower heat flux near to the ends of the test probe create

lower, or non-existent, fouling as can be seen in Fig. 2. The simulation conditions for Fig. 9 are the same as those given in the caption to Fig. 4.

Table 2. Experimental Validation of CFD Predicted Thermocouple Temperatures

	Measured	Predicted	Conditions
T_{ws}	636 K	638 K	Crude A; 81kW/m ² ; 200rpm
T_{wb}	647 K	644 K	Crude A; 81kW/m ² ; 200rpm
T_{ws}	651K	649.5 K	Crude B;106kW/m ² ; 200rpm
T_{wb}	664 K	662.5 K	Crude B;106kW/m ² ; 200rpm

In addition to the velocity and temperature fields, the Comsol simulation provides solutions to the turbulent velocity field and velocity gradients from which the shear stress distribution can be obtained. Figure 11 shows the shear stress distributions along the heated probe surface as a function of the stirrer speed for a power of 500W and heat flux of 106 kW/m². As expected, the surface shear stress on the heated probe surface is reduced as the stirrer speed is reduced. The solid line in Fig. 11 is for 400 rpm (6.67 Hz), the chain line for 200 rpm (3.33 Hz), and the dotted line for 100 rpm (1.67 Hz).

The curves in Figs. 9, 10, and 11 show data from the top of the heated probe ($z = 0$) to its shoulder at the bottom ($z = 0.07m$). The fact that the thermocouples are distributed circumferentially does not matter because it has been shown that the axially symmetrical 2-D simulation is an excellent approximation, and hence the data are independent of the circular coordinate ϕ .

For the purposes of comparison, the CFD simulation was also carried out for the Crude B flowing inside a standard tube of 14.84 mm internal diameter. Flow was assumed to be fully developed and turbulent. The physical properties of the fluid and the bulk temperature were set to be the same as those used in the batch stirred cell simulation.

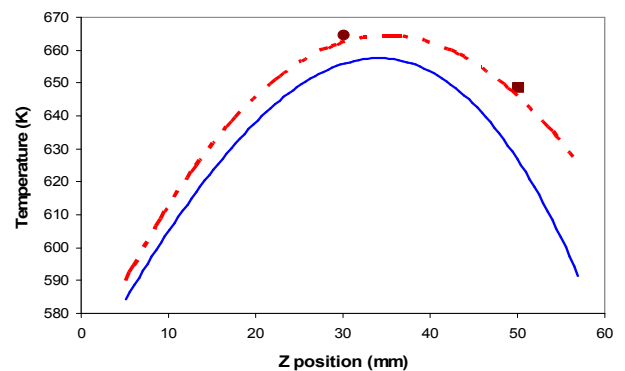


Fig. 9 Temperature distribution along the probe surface

Table 3 compares the simulation results for the shear stress at different linear velocities in the tube with those over the probe surface at various stirring speeds. Each line in the table is for a given value of shear stress. The shear stress for the inner surface of the tube is set equal to the

shear stress of the heated probe at its middle position. The Table reveals that a stirring speed of 400 rpm (6.67 Hz) would give a shear stress which is comparable to that in the tube operating under a typical refinery preheat train linear velocity of 2 m/s.

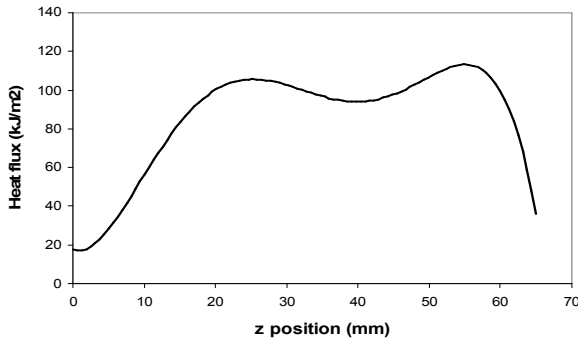


Fig. 10 Heat flux along the probe surface

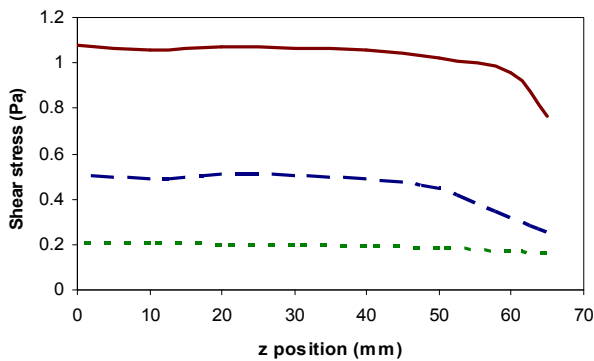


Fig. 11 Shear stress along the probe surface

Table 3 Shear stress comparison

Shear Stress (Pa)	Stirring Speed in the Cell (rpm)	Linear Velocity in Tube (m/s)	Re (Tube flow)
0.20	100	0.7	10388
0.52	200	1.3	19292
1.17	400	2.0	29680

As described earlier, the fouling rate in the batch stirred cell depends on the stirring speed and hence on the shear stress when the surface temperature is kept the same. An increase in the stirring speed from 200 to 400 rpm increases the shear stress from 0.52 Pa to 1.17 Pa and causes the fouling rate to be reduced from 0.016 m²K/(kWh) to 0.0054 m²K/(kWh). Crittenden et. al. (2009) reported that the linear fouling rate of Maya crude oil in a 14.8mm ID tubular test rig increased with an increase in the linear velocity up to 2 m/s. The fouling rate then decreased with further increases in the linear flow velocity. The shear stress condition in the tubular system at a linear velocity of 2 m/s would have been similar to that in the stirred cell at the stirring speed of 400rpm, as shown in Table 1. However, to date, no experimental data have been obtained in the present study with a stirring speed above 400 rpm.

The Comsol prediction of shear stress ought to be validated against experimental measurements. Unfortunately, no viable techniques for this measurement have been found to date.

Fouling Layer Thickness Profile

The fouling layer thickness on the probe was measured using the Proscan 2000. Starting from the top of the probe, the fouling zone for the conditions given in the caption of Fig. 4 was found to start at 8mm from the top and end at about 55 mm (in the manner shown in Fig. 2). Figure 12 shows the experimental fouling layer thickness profile. The profile was smoothed by means of a moving average in order to remove some coarse noise. The fouling layer was an accumulation of deposit obtained over a number of days.

Thorough drying of the probe was found to be critical in order to obtain a reliable scan result. Proper cleaning of a spot on the probe surface was also important in order to establish a reference value. A suitable sample rate for the scan was selected through a trial and error procedure.

The CFD predicted temperature profile over the probe surface is also plotted in Fig. 12 and can be compared with the deposit thickness profile. The scan rate was 300/second. The conditions are those described in the caption to Fig. 4. It can be seen that the fouling layer thickness profile over the probe surface is strikingly similar in form to the temperature profile, with their maxima occurring near to the middle of the heated probe surface. As shown in Fig. 11, the shear stress over the probe surface where the fouling zone is located was relatively constant. Hence the fouling behaviour is solely determined by the surface temperature since the shear stress is more-or-less constant. Accordingly, the similarity of the temperature and the fouling layer thickness profiles can be used to explain qualitatively the fouling behaviour in the experiment.

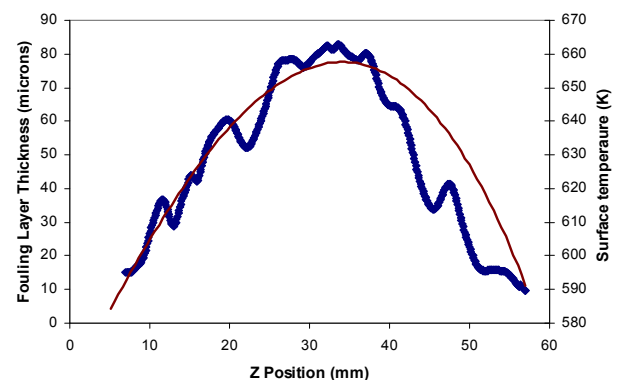


Fig. 12 Fouling layer thickness and simulated surface temperature profiles (blue: fouling layer thickness by Proscan; red line: surface temperature by Comsol simulation)

Arrhenius plot

Given the near linear fouling rate after the end of the induction period (Figure 3) and the same running time regardless of the position on the probe surface, the fouling rate at a given position can be expressed in terms of the

fouling layer thickness at any given position. The Arrhenius plot can now therefore be taken in terms of logarithm of the fouling layer thickness, x , as a function of the inverse of the absolute surface temperature, T :

$$\ln x = A - E_A/RT \quad (10)$$

Here, A is the pre-exponential factor and E_A is the apparent activation energy, as described by Bennett et. al. (2009) and Crittenden et. al. (2009). The Arrhenius plot is shown in Fig. 13 from which the apparent activation energy of 60.7 kJ/mol can be obtained for Crude B subjected to a power of 500W, an average heat flux of 106 kW/m² and a bulk temperature of 260°C over 33 hours of total running time in the batch stirred cell.

Unlike the more usual Arrhenius plots obtained for fouling experiments, this Arrhenius plot (Fig. 13) is in a continuous form, demonstrating the clear advantage of using the batch stirred cell in conjunction with both the Comsol simulation for surface temperature and the Proscan technique for deposit thickness. In most other crude oil fouling experiments, a minimum of three to four separate experiments at different surface temperatures need to be carried out in order to obtain a few points to construct an Arrhenius plot. With the present fouling layer thickness approach, all the operational parameters are virtually subject to the same operational conditions and hence there can be no problem in reproducibility from run to run that is often found in more conventional fouling studies where several runs have to be completed in different time periods, a problem which is exacerbated if the same batch of crude oil is used from run to run. With the batch stirred cell system, the correlation between fouling layer and surface temperature is derived based on the natural distribution of the surface temperature and fixed shear stress. This should improve the reliability of the Arrhenius plot.

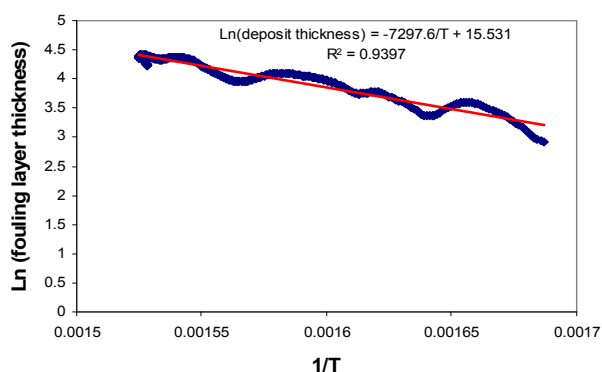


Fig. 13 Arrhenius plot for Petronas B crude oil (Blue: log of measured fouling layer thickness in microns against 1/T in K; Red line: Linear plot)

CONCLUSIONS

1. CFD and heat transfer simulations for a batch stirred cell system have been carried out using Comsol and validated partially against the measured temperature data at various axial positions on the heated test probe.

The surface temperature and shear stress profiles which are predicted by the CFD model can be used to correlate successfully the fouling behaviour in the batch stirred cell system. The 2-D axial symmetry simplification has been justified by comparison with the 3-D simulation.

2. The Proscan technique is a viable technique for the measurement of fouling layer thickness profiles over the probe surface. Hence, it becomes possible to correlate, for a relatively fixed surface shear stress, the local fouling rate against the local surface temperature, and hence to obtain an Arrhenius plot from one experimental run. This approach significantly enhances the application potential of the simple batch stirred cell fouling test system.
3. The CFD predicted shear stress data may need to be validated against viable experimental measurements.
4. The stirred batch cell apparatus is not restricted to use with crude oils and may be adapted easily for experiments on other systems such as scaling.

ACKNOWLEDGEMENTS

The authors are grateful to the UK's Engineering and Physical Sciences Research Council (EPSRC) for the award of a research grant (EP/D506131/1) to study the role of asphaltenes in crude oil fouling. The authors are grateful also to their EPSRC project partners at Imperial College London and the University of Cambridge, as well as to ExxonMobil and Petronas who supplied samples of crude oils.

NOMENCLATURE

- A pre-exponential factor
- C_p specific heat capacity, J/(K kg)
- C_μ model constant for modeling the turbulent viscosity
- $C_{\epsilon 1}$ parameter in k- ϵ turbulence model
- $C_{\epsilon 2}$ parameter in k- ϵ turbulence model
- E_a activation energy, kJ/mol
- k turbulent kinetic energy, m²/s²
- k_{eff} effective thermal conductivity, W/(K m)
- k_o molecular thermal conductivity, W/(K m)
- k_T turbulent thermal conductivity, W/(K m)
- R universal gas constant, 8.314 J/mol K
- R_f fouling resistance, m² K/kW
- T absolute temperature, K
- t time, s
- u flow velocity, m/s
- x fouling layer thickness, m
- z vertical position from the probe top, mm
- ϵ turbulent kinetic energy dissipation rate, m²/s³
- η dynamic viscosity, Pa.s
- η_T turbulent dynamic viscosity, Pa.s
- ρ density, kg/m³
- σ_ϵ turbulent Prandtl number for ϵ in k- ϵ turbulence model
- σ_k turbulent Prandtl number for k in k- ϵ turbulence model

REFERENCES

- Asomaning, S. and Watkinson, A. P., 2000, Petroleum stability and heteroatom species effects in fouling of heat

exchangers by asphaltenes. *Heat Transfer Engineering*, Vol. 21, pp. 10-16.

ASTM D341, 2003, Standard test method for viscosity-temperature charts for liquid petroleum products, ASTM International.

Bennet, C. A., Kistler, R. S., Nangia, K., Al-Ghawas, W., Al-Hajji, N. and Al-Jemaz, A., 2009, Observation of an isokinetic temperature and compensation effect for high temperature crude oil fouling, *Heat Transfer Engineering*, Vol. 30 (10-11), pp.794-804.

Churchill, S. W., 1988, *Viscous Flows: The Practical Use of Theory*, Butterworths, Boston, pp118-119.

Comsol, 2006a, Model library - chemical engineering module, pp. 238-240.

Comsol, 2006b, Model library - chemical engineering module, pp. 230-231.

Crittenden, B. D., Kolaczowski, S. T. and Phillips D. Z., 2009, Crude oil fouling in a pilot-scale parallel tube apparatus, *Heat Transfer Engineering*, Vol. 30(10-11), pp. 777-785.

Eaton, P., 1983, Fouling test apparatus, US patent 4383438.

Eaton, P. and Lux, R., 1984, Laboratory fouling test for hydrocarbon feed-stocks, *ASME-HTD*, Vol. 35, pp. 33-42.

Mullin, T., Lorenzen, A. and Pfister, G., 1983, Transition to turbulence in a non-standard rotating flow. *Physics Letters A*, Vol. 96 (5), pp. 236-238.

Nelson, W. L., 1958, *Petroleum Refinery Engineering*, 4th edition, McGraw-Hill, New York, pp 169 and 530.

Smith, G. P. and Townsend, A. A., 1982, Turbulent couette flow between concentric cylinders at large Taylor numbers, *J Fluid Mech*, Vol. 123, pp. 187-217.

Wilcox, D. C., 2000, *Turbulence modeling for CFD*, 2nd edition, DCW Industries Inc, La Canada, CA, pp 123-127.

Young, A., Venditti, S., Berruoco, C., Yang, M., Waters, A., Davies, H., Millan, M. and Crittenden, B. D., 2009, Characterisation of crude oils and their fouling deposits, presented at 8th *International Conference on Heat Exchanger Fouling and Cleaning: Challenges and Opportunities*, Schladming, Austria, 14-19 June.